Integrated Power Modeling for a Solar-Powered, Computationally-Intensive Unmanned Aircraft

Or D. Dantsker,* Mirco Theile,† and Marco Caccamo ‡
Technical University of Munich, Garching, Germany

In recent years, we have seen an uptrend in the popularity of UAVs driven by the desire to apply these aircraft to areas such as precision farming, infrastructure and environment monitoring, surveillance, surveying and mapping, search and rescue missions, weather forecasting, and more. The traditional approach for small size UAVs is to capture data on the aircraft, stream it to the ground through a high power data-link, process it remotely (potentially off-line), perform analysis, and then relay commands back to the aircraft as needed. Given the finite energy resources found onboard an aircraft (battery or fuel), traditional designs greatly limit aircraft endurance since significant power is required for propulsion, actuation, and the continuous transmission of visual data. All the mentioned application scenarios would benefit by carrying a high performance embedded computer system to minimize the need for data transmission. A major technical hurdle to overcome is that of drastically reducing the overall power consumption of these UAVs so they can be powered by solar arrays, and for long periods of time. This paper describes an integrated power model for a solar-powered, computationally-intensive unmanned aircraft that includes power models for solar generation, aircraft propulsion, and avionics. These power consumption and generation models are described, derived, and integrated into a cohesive system-wide aircraft power model that is presented in the form of a systemic flow diagram. Power balance expressions are also imposed based on temporal and physical constraints. Compared to works in the existing literature, the integrated model presented follows a holistic approach for UAV modeling that encompasses aircraft, propulsion, and solar models under realistic assumptions. Additionally, in order to enable high fidelity estimation while requiring minimal computation power, the model was developed to estimate the power consumption and generation based on flight path state, without needing precise aerodynamic measurements, e.g. angle-of-attack. Several of the methods have already been evaluated by means of ground and flight testing, as well as simulation, and showed errors ranging from negligible to approximately 5%. The motivation behind this work is the development of computationally-intensive, long-endurance solar-powered unmanned aircraft, the UIUC Solar Flyer, which will have continuous daylight ability to acquire and process high resolution visible and infrared imagery. Therefore, having a holistic integrated power model that can encompass power generation and consumption allows further aircraft and mission design and optimization can be performed.

Nomenclature

CPP	=	coverage path planning
CPU	=	central processing unit
ESC	=	electronic speed controller
FoV	=	field of view
GaAs	=	gallium arsenide
GPU	=	graphics processing unit
MPPT	=	maximum power point tracker
NREL	=	National Renewable Energy Laboratory
RPM	=	rotations per minute
SPA	=	Solar Position Algorithm
UAV	=	unmanned aerial vehicle

*Researcher, Department of Mechanical Engineering, or.dantsker@tum.de
†Ph.D. Student, Department of Mechanical Engineering. mirco.theile@tum.de
‡Professor, Department of Mechanical Engineering, mcaccamo@tum.de

$\vec{a}$	=	aircraft acceleration vector
A_{array}	=	solar array area
ΔA	=	unprocessed area per time
b	=	wingspan
c	=	wing mean chord
C_D	=	drag coefficient
C_{D_i}, C_{D_o}	=	induced and parasitic drag coefficients
C_L	=	lift coefficient
C_P	=	power coefficient
C_T	=	thrust coefficient
D	=	propeller diameter, drag
$E_{battery}$	=	battery energy
$E_{battery,max}$	=	battery energy capacity
f_r	=	frame rate
F	=	frames per pixel/feature
F_{min}	=	min allowable frames per pixel/feature
$\vec{F}$	=	force vector
g	=	gravitational acceleration
h	=	altitude
h_{max}	=	altitude constraint by p_{min}
i_m	=	motor current
i_0	=	zero load motor current
I_{solar}	=	solar flux
ΔI	=	information gain per time
J	=	advance ratio
K	=	aerodynamic constant
K_i, K_p	=	propulsion model constants
K_v	=	motor speed constant
L	=	lift force
L/D	=	lift-to-drag ratio
$\mathscr{L}$	=	computational load
$\mathscr{L}_{flight}$	=	flight control computational load
$\mathscr{L}_{mission}$	=	mission computational load
m	=	aircraft mass
n	=	propeller and motor rotation rate
o_y	=	minimal overlap ratio
p	=	ambient pressure, spacial resolution
p_{min}	=	minimum spacial resolution
p_x, p_y	=	image resolution in principle axis
P	=	power
$P_{avionics}$	=	avionics power consumption
$P_{battery}$	=	battery power (output positive)
$P_{computation}$	=	computation power consumption
P_{dyn}	=	dynamic power
P_{ESC}	=	ESC output power
P_{FM}	=	flight mechanics power
P_{in}	=	input power to power bus
P_{motor}	=	motor output power
P_{other}	=	other device power consumption
P_{out}	=	output power from power bus
$P_{propulsion}$	=	propulsion power consumption
P_{sensor}	=	sensor power consumption
P_{shaft}	=	shaft output power
$P_{soaring}$	=	soaring power generation
P_{solar}	=	solar array power generation
P_{ss}	=	steady state power
P_{thrust}	=	aerodynamic thrust power from propeller
q	=	dynamic pressure
Q	=	torque
r	=	image aspect ratio
R	=	universal gas constant
R_m	=	internal motor resistance
S	=	wing area
t	=	time, ambient temperature
t_o	=	initial time
T	=	thrust, current time
T_{ss}	=	steady state thrust
$\hat{u}_{array}$	=	solar array unit direction
$\hat{u}_{sun}$	=	sun ray unit direction
U_{emf}	=	motor back emf voltage
U_m	=	motor terminal voltage
v	=	velocity
v_{max}	=	max allowable velocity for F_{min}
$\vec{v}$	=	velocity vector
w	=	solar array normal direction
W	=	weight
x,y	=	lengths in principle axis
Δx,Δy	=	distance travelled between frames
Δy_{min},Δy_{max}	=	min/max allowable distance between frames
α	=	field of view angle
$\chi(P_{battery})$	=	battery efficiency (piece-wise)
γ	=	climb angle
η_{array}	=	solar array angular efficiency
$\eta_{battery,in}$	=	battery charging efficiency
$\eta_{battery,out}$	=	battery discharing efficiency
η_{ESC}	=	ESC efficiency
η_{motor}	=	motor efficiency
$\eta_{propeller}$	=	propeller efficiency
η_{solar}	=	solar array/cell conversion efficiency
ϕ	=	roll (bank) angle
ρ	=	density of air
$\theta_{sun-array}$	=	relative sun-array angle

I. Introduction

In recent years, we have seen an uptrend in the popularity of UAVs driven by the desire to apply these aircraft to areas such as precision farming, infrastructure and environment monitoring, surveillance, surveying and mapping, search and rescue missions, weather forecasting, and more. The traditional approach for small size UAVs is to capture data on the aircraft, stream it to the ground through a high power data-link, process it remotely (potentially off-line), perform analysis, and then relay commands back to the aircraft as needed.[1–3] Given the finite energy resources found onboard an aircraft (battery or fuel), traditional designs greatly limit aircraft endurance since significant power is required for propulsion, actuation, and the continuous transmission of visual data. All the mentioned application scenarios would benefit by carrying a high performance embedded computer system to minimize the need for data transmission. A major technical hurdle to overcome is that of drastically reducing the overall power consumption of these UAVs so that they can be powered by solar arrays. The process of reducing aircraft power consumption is required to reduce the aircraft weight, prolong flight time, and ultimately reduce cost in order to support the widespread adoption of UAVs for different types of missions. In order to do so, the power requirement of an aircraft and the conversion efficiencies of its various systems must be modeled and parametrized.

Currently, the UIUC-TUM Solar Flyer, which is shown in Fig. 1, is in development to enable a variety of all-daylight hour missions to be performed, involving continuous acquisition and processing of high resolution visible and infrared imagery. The aircraft is instrumented with an integrated autopilot, the uavAP autopilot,[4] and high-fidelity data acquisition system with an integrated 3D graphics processing unit (GPU). In order to keep the aircraft relatively inexpensive, both in labor and cost, the aircraft has been developed using a majority of commercial-off-the-shelf components, which therefore highly limits the number of viable options. The airframe chosen for development was selected through trade studies [5] that considered airframe availability and payload requirements as well as potential energy collection — more detail regarding airframe selection and integration can be found in related literature.[5–7] In similar recent related work, a propulsion system optimization tool was developed and validated[8] and then applied to the UIUC-TUM Solar Flyer.[9]

Figure 1: The UIUC-TUM Solar Flyer aircraft.

However, a key resource going forth in the development of the aircraft is the formulation of a holistic integrated power model that can encompass power generation and consumption such that further aircraft and mission design and optimization can be performed. Previous works have separately looked at electric aircraft modeling,[10–13] solar aircraft modeling,[14–18] and propulsion system modeling[19–26] with varying degrees of assumptions. Similarly, others have also looked into aircraft dynamics modeling for the purpose of creating accurate simulation.[27–30] Compared to works in the existing literature, the model presented follows a holistic approach for UAV modeling that encompasses aircraft, propulsion, and solar models under realistic assumptions.

This paper will first provide an overview of the integrated power model. This will include a system-wide flow diagram of the power model, a description of the aircraft elements included, and power balance equations. Then the paper will present solar power generation models. This will be followed by an aircraft propulsion power consumption model. After that, an avionics power consumption model will be presented. Finally, a summary will be given and future work will be discussed.

II. Power Model Overview

An integrated power model was developed for a long-endurance, solar-power type aircraft, such as the UIUC-TUM Solar Flyer. The integrated model, which is visualized in Figure 2, provides a complete system-level mathematical description from which future power-aware aircraft design, integration, and optimization can be made. The core elements of this model are power generation, power consumption, power distribution, and energy storage.

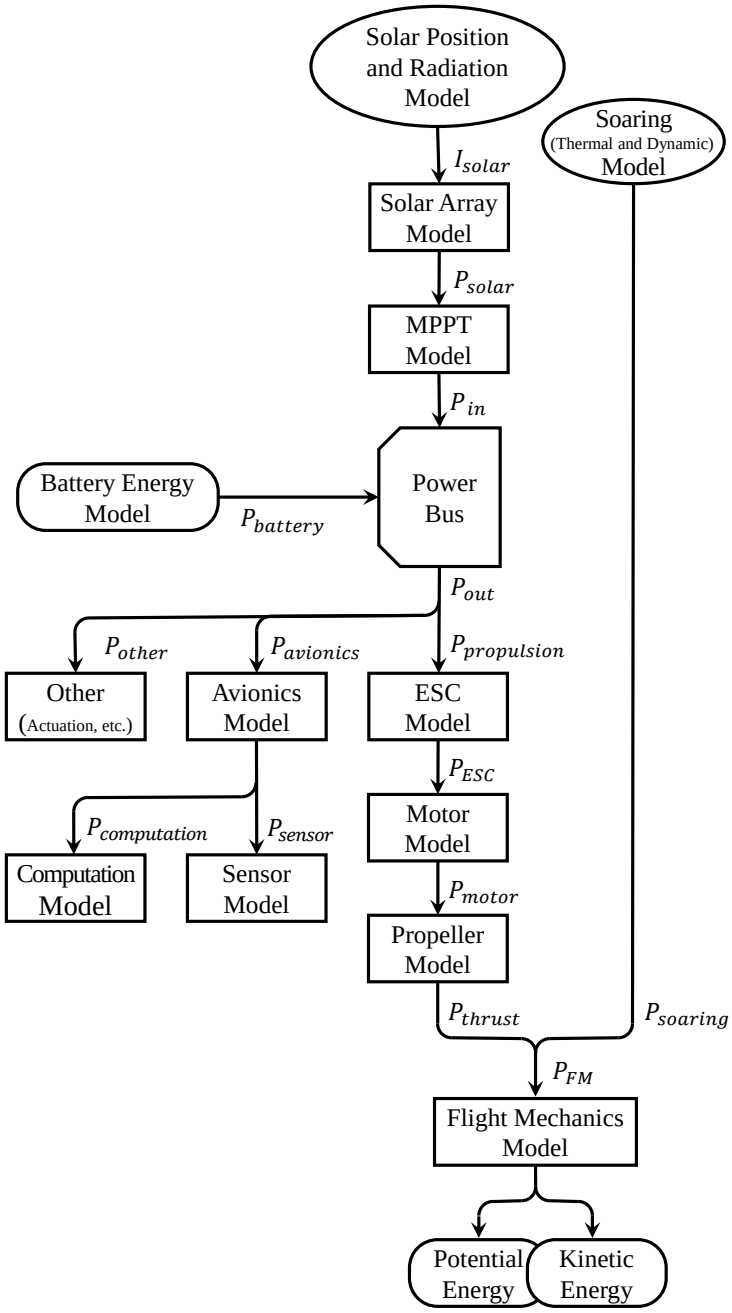

Figure 2: Diagram of the integrated power model for a long-endurance, solar-power type aircraft.

A. Power Elements

Power generation elements modeled in the integrated aircraft power model include a solar position and radiation model, a solar array model, and maximum power point tracker (MPPT) solar charge controller model. These elements are addressed in Section III. The integrated aircraft power model also enables integration of soaring harvested from thermal updrafts and wind shear, i.e. thermal and dynamic soaring. However, specific modeling techniques for power collection through soaring will not be included in the scope of the current work – there are many that can be found in existing literature.[31–36]

In terms of power consumption, elements are categorized into propulsion, avionics, and other; these are addressed in Sections IV and V. Propulsion power is computed using an flight mechanics model, thrust model, motor model, and a electronic speed controller (ESC) model. The avionics power is computed from the baseline and flight conditions of the avionics components, which include the flight control and data acquisition system, the computational platform, and the sensors. Other power consuming elements include such components as actuators and navigation lights.

Power distribution onboard the aircraft is handled by a power bus, which for the purpose of this work is assumed to be transparent, i.e. no losses are incurred in transmission through the power bus. Finally, energy storage is stored in two forms: electrical/chemical energy in the form of batteries and through mechanical energy in the form of aircraft potential and kinetic energy.

B. Power Balance

In order to enable long-endurance flight, temporal power balance must be maintained. Specifically, that the amount of power that is being consumed over time is less than that available from solar power collection sources and the battery. Thus, at the power distribution bus in Figure 2, it must always hold that,

$$0 = P_{out}(t) - P_{battery}(t) - P_{in}(t), \quad \forall t \in [t_0, T] \tag{1}$$

with t_0 being the time of take-off and T being the time of landing. Note that positive battery power $P_{battery}$ signifies the outward flow of power from the battery, i.e. the battery is being discharged. Conversely, negative battery power signifies power flowing into the battery, i.e. the battery is being charged.

Additionally, it must be imposed that the battery may only hold energy equivalent to less than or equal to its energy capacity,

$$0 \leq \int_{t_0}^{t} \chi(P_{battery}) \cdot P_{battery}(s)ds + E_{battery}(t_0) \leq E_{battery,max}, \quad \forall t \in [t_0, T] \tag{2}$$

in which

$$\chi(P_{battery}) = \begin{cases} \eta_{battery,in} & \text{if } P_{battery} < 0 \\ \frac{1}{\eta_{battery,out}} & \text{if } P_{battery} \geq 0 \end{cases} \tag{3}$$

The above equation effectively defines limitation of the battery's ability to retain and store energy within its capacity limits and takes into account efficiency losses of charging ($\eta_{battery,in}$) and discharging ($\eta_{battery,out}$) the battery. Since $P_{battery}$ is measured at the bus, $\frac{1}{\eta_{battery,out}} \cdot P_{battery}$ is drawn from the battery when discharging. It should be noted that for the cases where the battery is fully charged and excess power is being generated and not used, i.e. $P_{out} < P_{in}$, the excess power will not be rejected in the form of heat being shed from the solar arrays.

III. Solar Power Generation

In order to maintain a sufficient energy buffer, it is important to balance energy consumption with energy generation. Therefore, developing a high-fidelity model for solar power generation is vital for the continued operation of a long-endurance, solar-powered unmanned aircraft. Solar-power generation will vary based on physical phenomena, i.e. solar position and radiation, and the performance of aircraft hardware components, i.e. the solar array and MPPT charge controller. Models for solar position and radiation and for the solar array are described below. For the scope of this work, MPPT charge controllers are simply assumed to have fixed efficiency loss, as commonly described in the literature.[16,22,26,37]

A. Solar Position and Radiation Model

The solar potential of an energy harvesting component depends on two external factors, the position of the sun, thereby yielding the direction of the sun rays, and the radiation, thereby yielding flux that can be harvested. These factors have been studied for many years and are well parameterized and modeled.[38–42]

A standard source for determining the position of the sun is the U.S. Department of Energy, National Renewable Energy Laboratory (NREL) Solar Position Algorithm (SPA).[43] The NREL SPA allows for calculation of the zenith and azimuth angles of the sun based on the date, time, and location on Earth with uncertainties of +/- 0.0003 degrees for the years of -2000 to 6000. The relative position of the sun is then used to calculate the incidence between the solar array direction and the sun rays; this is used further in the following subsection.

There are many ways to estimate solar radiation, i.e. solar flux, available for harvesting. Similarly to the position of the sun, the quantity of available solar flux depends on date, time, and location, however, the quantity of solar flux also depends on atmospheric conditions such as cloud amount and layering, precipitation, fog/smoke, etc.[44] There are many sources that outline different methods to estimate solar flux as well as provide libraries to calculate solar flux.[45,46] Many works in the literature also estimate solar flux using random distributions.[36]

B. Solar Array Model

Solar arrays' energy production relies on the ability to convert solar radiation into electrical energy. The effectiveness of this energy conversion process depends on two factors: conversion efficiency and off-angle performance. These factors are analogous and depend on the factors affecting solar potential.

The first major factor that affects the performance of solar array is the conversion efficiency of the cells. This efficiency is dependent on the chemistry and design of the photo-voltaic cells being used. Specifically, the factors affecting solar cell efficiency are reflectance, thermodynamic efficiency, charge carrier separation efficiency, charge carrier collection efficiency, and conduction efficiency values. Therefore, the choice of photo-voltaic cell directly influences the resulting efficiency of the solar array. The efficiency of a given photo-voltaic cell is affected by external factors such as ambient temperature, spectrum, and flux. Therefore, cell efficiency is often modeled as either a variable of the aforementioned factors or a single value based on the dominant conditions. For example, the Alta Devices single-junction GaAs photo-voltaic cells[47] used on the UIUC-TUM Solar Flyer, are specified to be 26% efficient at an air mass of 1.5 and 1000 W/m^2 at 25 degrees Celsius, however are only 23% efficient at an air mass of 1.0 and 1366 W/m^2, also at 25 degrees Celsius; additionally, these cells are said to decrease in efficiency as they are heated. Thus, due to the dominant environmental conditions expected for the UIUC-TUM Solar Flyer to operate in, i.e. 1000 W/m^2 at approximately 25 degrees Celsius, the Alta Devices single-junction GaAs photo-voltaic cells were modeled as having a constant efficiency of $\eta_{solar} = 26\%$; this was supplemented by experimental measurements that verified solar array performance.

The second major factor that affects the performance of solar array is off-angle performance. More often than not, solar arrays are not oriented normal to the direction of the sun rays and thus only receive solar radiation equivalent to the flux multiplied by the projected area:

$$P_{solar} = (I_{solar}\hat{\mathbf{u}}_{\mathbf{sun}}) \cdot (A_{array}\hat{\mathbf{u}}_{\mathbf{array}})\eta_{solar} \tag{4}$$

From the geometric definition of a dot product,

$$\hat{\mathbf{u}}_{\mathbf{sun}} \cdot \hat{\mathbf{u}}_{\mathbf{array}} = \cos(\theta_{sun-array}) \tag{5}$$

However, as solar cells do not have ideal off angle performance, the above expression must be re-written with a function of relative angles between the array direction and the sun rays, $\eta_{array}(\theta_{sun-array})$. Thus,

$$P_{solar} = I_{solar}A_{array}\eta_{solar}\eta_{array}(\theta_{sun-array}) \tag{6}$$

For the aforementioned Alta Devices single-junction GaAs photo-voltaic cells, the off-angle performance follows the cosine of the angle up to approximately 45 degrees, after which it drops off slightly. Experimental measurements[5] as well as a 2nd-order polynomial fit are compared to the cosine of the angle in Figure 3.

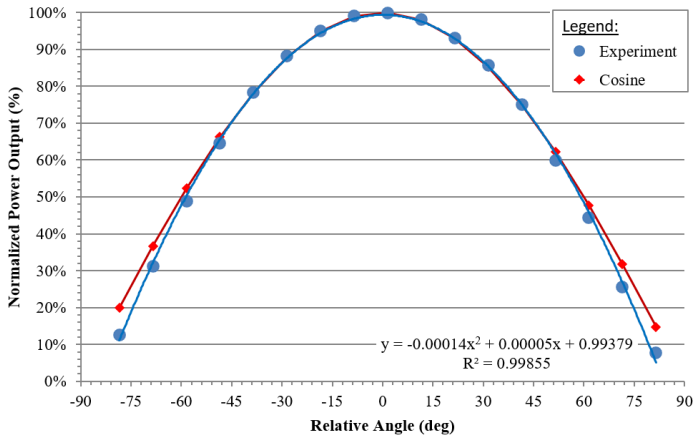

Figure 3: Angular performance data for the Alta Devices single junction GaAs solar cells.

However, determining the relative orientation of the aircraft solar arrays with respect to the sun rays is complicated in that the aircraft is continually moving and often reorienting, and that the solar arrays are hardly oriented in a single flat plane. Specifically, these complications depend on the aircraft's geometry, orientation, and wing flex. An example aircraft geometry, with the solar array normal vectors being offset from the aircraft reference normal, can be visualized in Figure 4 for the UIUC-TUM Solar Flyer; knowledge of such geometry allows the baseline angular offset to be calculated. Meanwhile, to determine aircraft orientation, the aircraft trajectory is used to directly output bank, i.e. roll angle, and climb angle. Using the trajectory, the expected load factor can be estimated based on the curvature, which knowing the aircraft's lift curve slope, allows angle-of-attack to be computed. The aircraft pitch angle can then be determined from the angle-of-attack and climb angle. Similarly, wing flex will be estimated based on aircraft loading, which can be ascertained from aircraft trajectory state. The advantage of this method is that neither angle-of-attack nor aircraft loading need to be directly measured.

Therefore, for aircraft with n solar arrays with identical conversion and angular performance,

$$P_{solar} = I_{solar}\eta_{solar}\sum_{i=1}^{n} A_{array_i}\eta_{array}(\arccos(\hat{\mathbf{u}}_{\mathbf{sun}} \cdot \hat{\mathbf{u}}_{\mathbf{array_i}})) \tag{7}$$

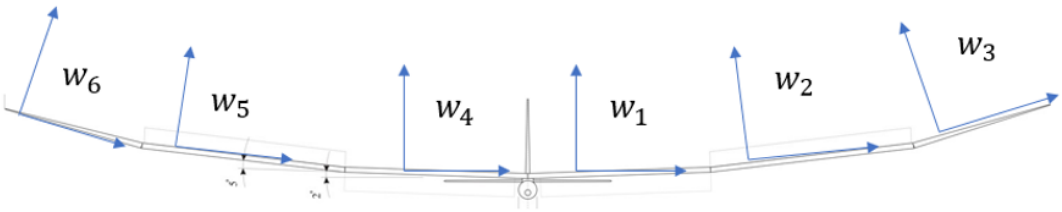

Figure 4: Solar array orientations of the UIUC-TUM Solar Flyer.

IV. Aircraft Propulsion Power Consumption

On an electric UAV, there are a series of propulsion system power-consuming components. The below propulsion power model analytically explains how power flows from the energy source into thrust power. First, the energy source, e.g. battery or solar collection system, provide the propulsion power; electronic speed controller (ESC) routes the electric power via the wire leads to the motor poles in order to induce rotation with an efficiency loss; then, the motor converts the electric power into rotational power to drive the propeller, also with an efficiency loss; after that, the propeller converts the rotation power into thrust power, applying a forward thrust force to the aircraft - with an efficiency loss. Thus, the product of the propulsion power, ESC efficiency, motor efficiency, and propeller efficiency is the thrust power:

$$P_{propulsion} \cdot \eta_{ESC} \cdot \eta_{motor} \cdot \eta_{propeller} = P_{thrust} \tag{8}$$

In order to make the power consumption model as versatile as possible, state variable inputs are restricted to easily measurable values. Specifically, the variable inputs are properties of the aircraft maneuver, including velocity, acceleration, roll (bank) angle, and climb angle. Doing so requires certain assumptions[a], which will work well for the overwhelming majority of long-endurance UAV flight. Therefore, the power model provides an estimation based on the motion of the aircraft, i.e. flight path, with minimal knowledge of the aircraft flight mechanics attributes. Figure 5 shows how the model is cascaded from the input variables, through a flight mechanics model, a propeller model, a motor model, and an ESC model. This follows the high-level explanation mentioned above in Section II, similar to Figure 2, but in a backwards manner. It should be noted that for the purpose of the propulsion power derivation, thrust power P_{thrust} will be set equal to flight mechanics power P_{FM}, i.e. soaring power $P_{soaring}$ will temporarily be set to zero, as adjustments can easily be implemented by decreasing thrust power in Equation (8).

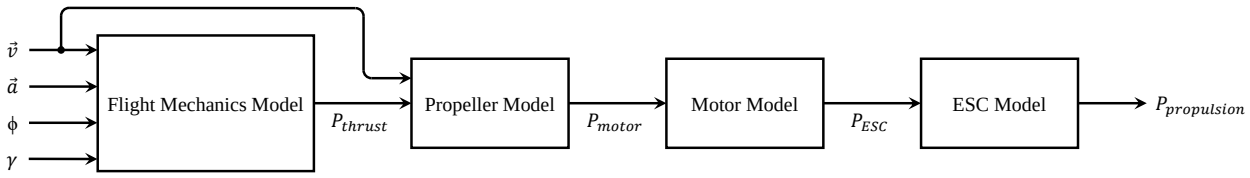

Figure 5: Aircraft propulsion power modeling based on aircraft state.

[a]It is assumed that the angle-of-attack remains relatively constant,the incidence angle is approximately zero, and thus the flight path climb angle is approximated as the measurable pitch angle. Additionally, it is assumed that there is minimal side-slip allowing for the turn radius to be calculated directly from the roll angle.

A. Flight Mechanics Model

The flight mechanics model takes into account power required for steady-state flight as well as dynamic maneuvers. Specifically, the total thrust power is given by

$$P_{thrust} = P_{ss} + P_{dyn} \tag{9}$$

The steady state power portion of the thrust power, P_{ss}, is calculated from steady-state maneuver data that can be measured or simulated, including velocity v, roll (bank) angle ϕ, and climb angle γ. Figure 6 shows these state variables applied to level, turning, and climbing flight [b]. The remainder of the steady state portion of the propulsion power model will be derived from elementary flight mechanics principles.[48] Assumptions of constant lift-to-drag ratio and of non-constant lift-to-drag ratio were made in a previous derivation set;[49] however, for the sake of brevity and accuracy, only the non-constant lift-to-drag ratio assumption derivation will be shown.

The steady state power is only valid for steady-state maneuvers and greatly differ from total thrust power in maneuvers that incorporate acceleration. However, it is still useful in calculating the total thust power in such maneuvers. To incorporate the dynamics into the power model, dynamics power, P_{dyn}, is added . The dynamic power is calculated based on Newton's second law

$$\vec{F}(\vec{a}) = m\vec{a} \tag{10}$$

and that power is equal to the dot product of force and velocity,

$$P(\vec{F},\vec{v}) = \vec{F}\cdot\vec{v} \tag{11}$$

Putting these expressions together gives the dynamic power as

$$P_{dyn}(\vec{a},\vec{v}) = m\,(\vec{a}\cdot\vec{v}) \tag{12}$$

It is assumed the effect of rotational accelerations are negligible. Additionally, the model can be extended to take into account constant wind as well as wind gusts by modifying $\vec{v}$ and $\vec{a}$ in the previous expressions.

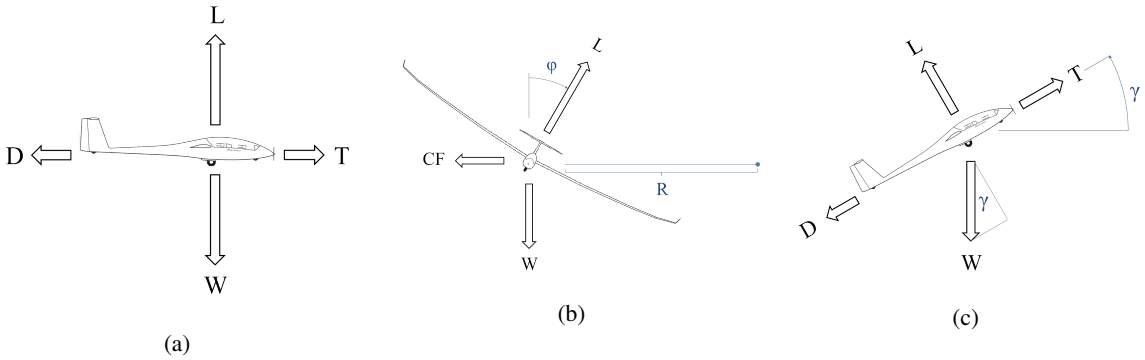

Figure 6: Steady-state forces on an aircraft in (a) level flight, (b) turning flight and (c) climbing flight.

For steady state flight to occur, there must be an equilibrium of forces and moments. As depicted in Figure 6a, there are four basic forces in level (cruise) flight: lift upward L, drag backward D, thrust forward T, and weight downward W. As these forces directly and solely oppose each other in equilibrium level flight, the magnitude of lift is equal to that of weight

$$L = W \tag{13}$$

where weight is equal to the aircraft mass multiplied by the gravitational acceleration

$$W = mg \tag{14}$$

[b] Note that based on the above stated assumptions, velocity is in the thrust direction.

And likewise the magnitude of thrust is equal to that of drag,

$$T = D \tag{15}$$

The ratio of the lift force to the drag force, the so called lift-to-drag ratio L/D, gives a measure of the aircraft design efficiency; again, for our purposes here, we will assume it is not constant.

In a level turn, shown in 6b, the airplane is rolled to a desired roll angle, ϕ. Due to the equilibrium of forces, the required lift force needs to be

$$L = \frac{W}{\cos\phi}. \tag{16}$$

Similar to the level turn, the steady-state power of climbing [or descending] flight can also be derived based on the equilibrium of forces. Figure 6c shows the schematics of a climb flight in which the airplane is flying with a climb angle γ. Balancing the forces yields the relation for thrust

$$T = D + W\sin\gamma \tag{17}$$

and the relation for lift

$$L = W\cos\gamma \tag{18}$$

In most cases, climbing and turning are performed separately so the above equations can be used individually; however, in some cases, both maneuvers are performed at the same time, resulting in a spiral flight. With the assumption that the lift-to-drag ratio is not constant and that a spiral is made up of a turn and a climb that influence each other, this information needs to be considered when solving for steady state propulsion power. Specifically, in order to define the spiral, Equations (16) and (18) are combined as

$$L = W\frac{\cos\gamma}{\cos\phi} \tag{19}$$

and Equation (17) is re-written as

$$D = T - W\sin\gamma \tag{20}$$

The expressions for lift and drag are introduced as

$$L = qSC_L \tag{21}$$

$$D = qSC_D \tag{22}$$

where S is the reference surface area, C_L and C_D are the lift and drag coefficients, respectively, and dynamic pressure q defined by

$$q = \frac{1}{2}\rho v^2 \tag{23}$$

Here, ρ is the air density. Therefore, the expressions for the lift coefficient is re-written as

$$C_L = \frac{2L}{\rho v^2 S} \tag{24}$$

The drag coefficient is defined as

$$C_D = C_{D_o} + C_{D_i} \tag{25}$$

where C_{D_o} is the parasitic drag coefficient at zero lift and C_{D_i} is the induced drag coefficient. The induced drag is expressed as a function of lift by

$$C_{D_i} = KC_L^2 \tag{26}$$

where K is a constant aerodynamic coefficient based on the wing platform shape[c]. Inserting Equation (26) into Equation 25 yields

$$C_D = C_{D_o} + KC_L^2 \tag{27}$$

[c] $K = 1/\pi eAR$, where e is the Oswald efficiency factor and AR is the wing aspect ratio.

and then inserting Equation (24) yields

$$C_D = C_{D_o} + \frac{4K}{\rho^2 S^2}\frac{L^2}{v^4} \tag{28}$$

Therefore, based on the expression for drag from above

$$D = \frac{1}{2}\rho S C_{D_o} v^2 + \frac{2K}{\rho S}\frac{L^2}{v^2} \tag{29}$$

Inserting Equation (19) for lift yields

$$D = \frac{1}{2}\rho S C_{D_o} v^2 + \frac{2KW^2}{\rho S}\frac{\cos^2\gamma}{v^2\cos^2\phi} \tag{30}$$

And setting the above equation equal to Equation (20) and inserting the equation for weight gives

$$T = \frac{1}{2}\rho S C_{D_o} v^2 + \frac{2Km^2g^2}{\rho S}\frac{\cos^2\gamma}{v^2\cos^2\phi} + mg\sin\gamma \tag{31}$$

Since power is the product of thrust and velocity

$$P_{ss} = \frac{1}{2}\rho S C_{D_o} v^3 + \frac{2Km^2g^2}{\rho S}\frac{\cos^2\gamma}{v\cos^2\phi} + mgv\sin\gamma \tag{32}$$

This expression can be simplified by assigning constants

$$P_{ss} = K_p v^3 + K_i\frac{\cos^2\gamma}{v\cos^2\phi} + mgv\sin\gamma \tag{33}$$

where

$$K_p = \frac{1}{2}\rho S C_{D_o} \tag{34}$$

$$K_i = \frac{2Km^2g^2}{\rho S} \tag{35}$$

It should be noted that these constants can be calculated from aircraft data; however, without pre-existing aircraft performance data, the constants are more easily determined from training data using linear regression with non-linear kernel.

B. Propeller, Motor, and ESC Models

With the calculated thrust power, the ESC, motor, and propeller efficiencies can now be incorporated to calculate the input power needed to produce this thrust. The relation is given by rearranging Equation (8)

$$P_{propulsion} = \frac{P_{thrust}}{\eta_{ESC}\cdot\eta_{motor}\cdot\eta_{propeller}} \tag{36}$$

where η_{ESC} is the ESC efficiency, $\eta_{propeller}$ is the propeller efficiency, and η_{motor} is the motor efficiency. The efficiency factors themselves depend on numerous factors that are directly or indirectly related to thrust and velocity as well as aircraft power system configuration, e.g. battery voltage.

There have been a variety of derivations developed for computing ESC efficiency.[10,19,20] These generally yield that ESC efficiency is a function of voltage and current. Duty cycle, which is proportional to shaft rotation rate and/or throttle input, is often also taken into account. For the scope of the current work, ESC efficiency will be fixed to a constant value, which is representative of its efficiency at cruise conditions, i.e. ESC efficiency curves have shown to flatten out once reaching a small percentage of their design operating current.[20]

1. Propeller

Propeller efficiency can be derived using blade element momentum theory (BEMT) and sectional airfoil theory as done in.[50] However, BEMT curves are highly sensitive to variation of the parameters used. In order to increase model accuracy, experimental data for propeller performance can be obtained from wind tunnel propeller testing[25,51] and/or an existing database,[52,53] with interpolation being done as required. Figure 7 provides example propeller performance polars for the Aeronaut CAM 13x6.5 propeller used on the UIUC-TUM Solar Flyer from 2017 to 2020. The process of determining the propeller efficiency for each given flight state follows the method presented in previous work.[8]

From the thrust, torque, rotation rate, and flow velocity values, the thrust coefficient, power coefficient, and propeller efficiency values are calculated. In order to perform these calculations, knowledge of the air density and propeller diameter is required. Using the temperature and pressure readings, the air density is determined using the equation of state

$$p = \rho R t \tag{37}$$

where R is the universal gas constant with a value for air of 287.0 $\mathrm{m}^2/\mathrm{s}^2/\mathrm{K}$ (1716 $\mathrm{ft}^2/\mathrm{s}^2/^\circ\mathrm{R}$).

The propeller advance ratio J is defined from the ratio of the measured air flow speed V to the propeller rotation rate n (in rev/s) and the propeller diameter D as

$$J = \frac{V}{nD} \tag{38}$$

The thrust coefficient C_T is calculated from the measured thrust T, rotation rate, air density, and the propeller diameter as

$$C_T = \frac{T}{\rho n^2 D^4} \tag{39}$$

In order to determine the power coefficient, propeller shaft output power P_{shaft} must be found. Propeller shaft power is determined from the measured torque Q and rotation rate by

$$P_{shaft} = 2\pi n Q \tag{40}$$

Therefore, the power coefficient C_P can be calculated from the measured rotation rate, propeller shaft power, air density, and propeller diameter as

$$C_P = \frac{P_{shaft}}{\rho n^3 D^5} \tag{41}$$

Finally, the propeller efficiency $\eta_{propeller}$ can be determined as

$$\eta_{propeller} = J\frac{C_T}{C_P} \tag{42}$$

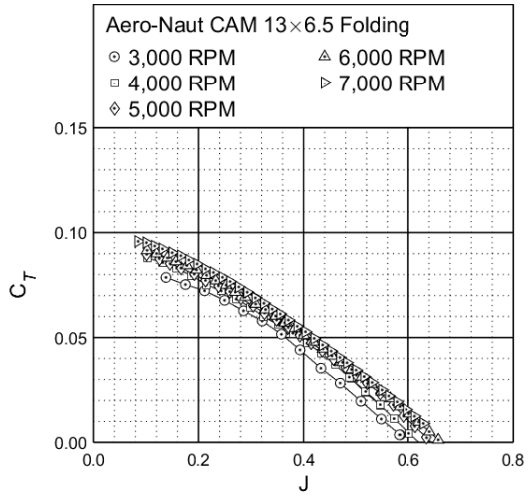

(a)

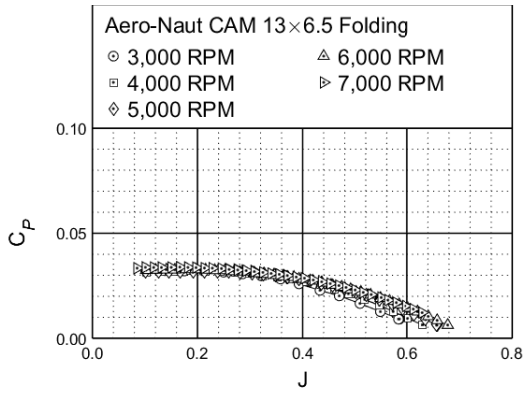

(b)

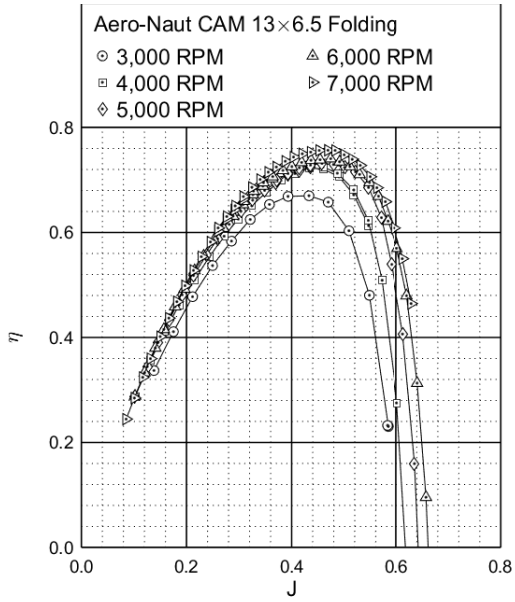

(c)

Figure 7: Propeller performance curves for the Aeronaut CAM 13x6.5 propeller used on the UIUC-TUM Solar Flyer from 2017 to 2020: (a) thrust (C_T), (b) power (C_P), and (c) efficiency $(\eta_{propeller})$ vs. advance ratio (J)

2. Motor

The motor efficiency is defined as the ratio between the shaft output power P_{shaft} and the motor input power P_{motor}.

$$\eta_{motor} = \frac{P_{shaft}}{P_{motor}} \tag{43}$$

The shaft output power P_{shaft} can be computed using Equation (40), however, the torque and rotation rate must be known. The rotation rate is either set or measured. Equations (40) and (41) are combined to determine the torque

$$Q = \frac{C_P \rho n^2 D^5}{2\pi} \tag{44}$$

Thus, it is assumed that the propeller rotation rate is set/measured and that the air density, propeller diameter, and propeller power coefficient are known. It should be noted that the power coefficient can be determined from performance curves with knowledge of current rotation rate and advance ratio (based on current velocity), both assumably set/measured.

Meanwhile, the motor input power P_{motor} is computed as the product of the motor voltage U_m and motor current i_m.

$$P_{motor} = U_m i_m \tag{45}$$

From modeling of brushed DC motors, which has been applied to brushless DC motors,[12] the voltage is found as

$$U_m = U_{emf} + i_m R_m \tag{46}$$

where U_{emf} is the back emf voltage and R_m is the motor internal resistance in Ohms. The back emf voltage is found by

$$U_{emf} = \frac{60n}{K_v} \tag{47}$$

where K_v is the motor speed constant in RPM (rev/min) per Volt.

The current is calculated from the torque from Equation (44)and two motor parameters

$$i_m = i_0 + \frac{2\pi K_v Q}{60} \tag{48}$$

where i_0 is the motor current at zero load in Amperes.

Alternately, other methods exist to determine motor efficiency. For example, a first order approximation by Drela[54] estimates motor efficiency as a function of motor voltage and rotation rate, and the 3 aforementioned motor parameters.

$$\eta_{motor}(n, U_m) = \left(1 - \frac{i_0 R_m}{U_m - 60n/K_v}\right) \frac{60n}{U_m K_v} \tag{49}$$

A second order approximation[55] also exists, however, it requires a fourth motor parameter, K_Q, the motor torque constant, which is not easily obtained from manufacturers but instead needs to be measured through dynamometer benchtop testing.[19]

3. *Propeller-Motor Rotation Rate and Efficiency Algorithm*

In order to determine the motor and propeller efficiencies, their rotation rate must be determined for each aircraft state. This calculation is performed using the equations presented in the above subsections that were arranged into *Rotation Rate and Efficiency Algorithm* and *Propeller Rotation Rate Subroutine* iterative technique; these can be visualized in Figs. 8 and 9, respectively, and are based on previous work.[8]

For each aircraft state the *Rotation Rate and Efficiency Algorithm* determines the rotation rate required for the propeller to achieve the desired thrust at the given velocity using the *Propeller Rotation Rate Subroutine*. It does so by iteratively running along the thrust coefficient curves on the propeller performance plots, finding points that produce the closest thrust coefficient values required to achieve the desired thrust, and then interpolating between curves; this is done using Equations (38) and (39). As mentioned earlier, the propeller performance curves can be attained from a variety of sources including experimentally-validated analytical methods,[56] BEMT results,[57,58] and wind tunnel data.[51–53]

Once the rotation rate is found for the propeller, the value is used to determine the shaft-to-thrust conversion efficiency of the propeller; this is done by interpolating the power coefficient for the propeller from its respective curves, and then using Equation (41). A specification-based analytical motor model, developed from the theory presented in Section IV.B.2, is then used to calculate the electric power-to-shaft power conversion efficiencies for the motor. This process is repeated for the motor and propeller for all aircraft states.

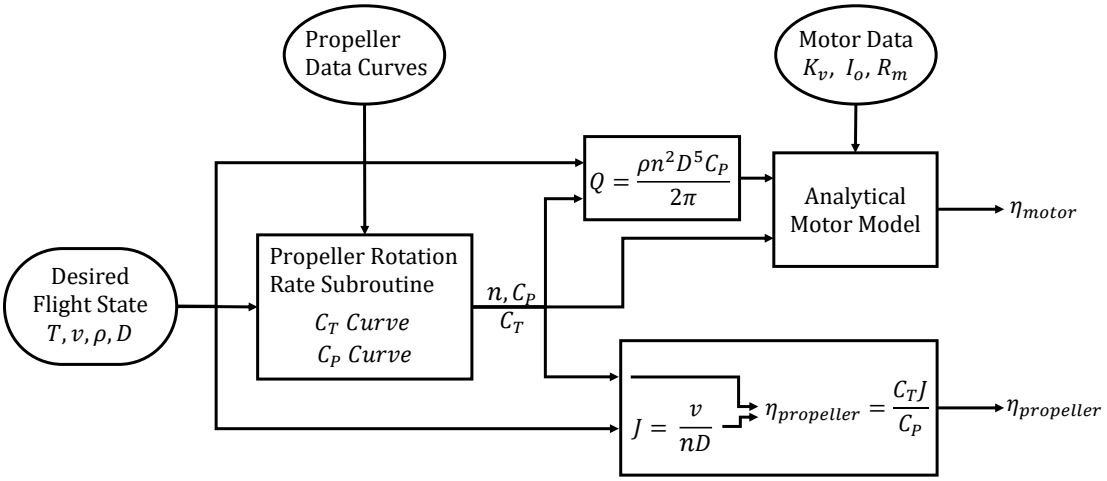

Figure 8: Process diagram of the *Rotation Rate and Efficiency Algorithm*.

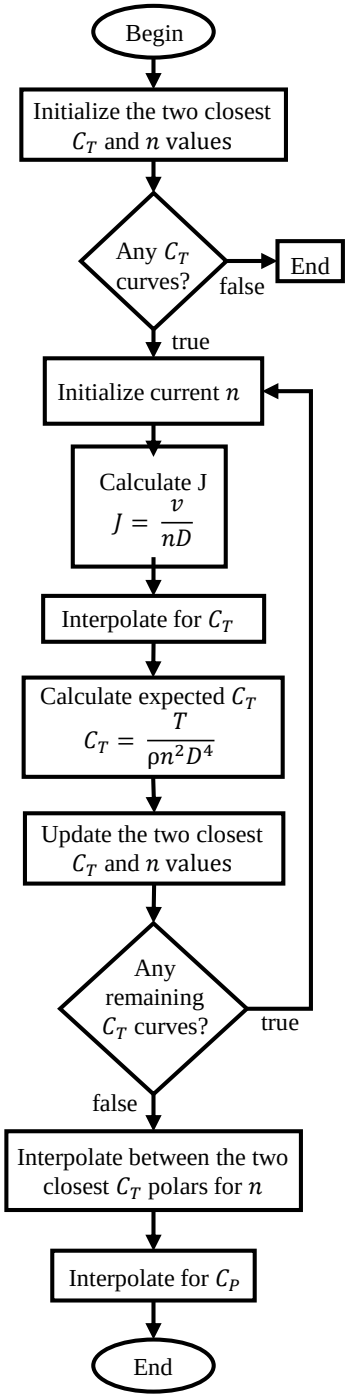

Figure 9: Process diagram of the *Propeller Rotation Rate Subroutine*.

C. Complete Propulsion Power Model

Combining the steady state and dynamic thrust power models and the propeller and motor models into a generic form yields

$$P_{propulsion}(\vec{v},\vec{a},\phi,\gamma) = \frac{P_{ss}(\vec{v},\phi,\gamma) + P_{dyn}(\vec{v},\vec{a})}{\eta_{propeller}\cdot\eta_{motor}\cdot\eta_{ESC}} \tag{50}$$

The final expression is

$$P_{propulsion} = \frac{K_p v^3 + K_i \frac{\cos^2\gamma}{v\cos^2\phi} + mgv\sin\gamma + m\vec{a}\cdot\vec{v}}{\eta_{propeller}\cdot\eta_{motor}\cdot\eta_{ESC}} \tag{51}$$

where K_p, K_i, and η_{ESC} were defined earlier and $\eta_{propeller}$ and η_{motor} are determined for each state using the *Rotation Rate and Efficiency Algorithm* and *Propeller Rotation Rate Subroutine*.

The aircraft propulsion power model was evaluated by means of flight testing using an existing, instrumented aircraft, which had extensively been used for avionics development as well as other purposes. The aircraft was autonomously flown through a reference flight path, which contained turns, climbs, descents, and straight line segments. The flight testing showed very close agreement between the power and energy estimates determined using the power model from aircraft state data and actual experimental power and energy measurements, within less than 5%.[8,49]

V. Avionics Power Consumption

The avionics power consumption is split between the power consumption of the sensors and computational unit(s). For this work, we consider sensor power consumption to be constant at $P_{sensors}$ while in operation. The power consumption of the computational units, $P_{computation}$, depends on the computational load of the embedded board. The computational load constitutes of two parts: the computational load due to flight control related computation, $\mathscr{L}_{flight}$, and the computations required for the mission, $\mathscr{L}_{mission}$. The computational load induced by the flight control algorithms can be assumed to be constant as the periodic computations of the uavAP autopilot and the Al Volo backend are mostly independent of the flight path. The computational load of uavAP can be measured within the uavEE[59] emulation environment.

For the UIUC-TUM Solar Flyer missions such as crop monitoring for precision agriculture or image stitching for environmental mapping can be formulated as coverage path planning (CPP) problems. Therefore, the derivation in this Section is for the mission power consumption of camera-based missions which require CPP. In addition to computational load modeling, constraints on maximum flight altitude and velocity can be derived within this context.

For the derivation, we assume that the video camera is mounted on a stabilizer which can correct for necessary attitude during flight, such as during roll maneuvers for turning. Additionally, we assume that the computational load of the mission algorithm is linear to the amount of information that is collected by the camera. Thus, to derive the computational load, the information flow of the camera has to be derived.

The derivation of the information flow has similarities with the system model described by Di Franco et al.[60] The relevant optical sensor characteristics are the Field of View (FoV) angle α, the image resolution (p_x, p_y), and the frame-rate f_r. We assume that the pixels are square and, thus, the aspect ratio r is defined as $r = \frac{p_x}{p_y}$. With these parameters, the recorded width x in meters can be calculated as follows:

$$x = 2\tan\left(\frac{\alpha}{2}\right)h, \tag{52}$$

with h being the altitude of the aircraft above ground level. The length y of the covered area can be calculated with the aspect ratio as $y = \frac{x}{r}$. Using the frame-rate parameter f_r, the traveled distance between frames can be expressed through

$$\Delta y = \frac{v}{f_r}, \tag{53}$$

with the aircraft speed v in the direction of y. From the resolution p_x and the area width x the spatial resolution

$$p = \frac{p_x}{x} \tag{54}$$

representing the pixels per distance can be calculated. The spatial resolution p and the advancement per frame Δy are used to calculate mission induced constraints on flight altitude h and velocity v.

A. Mission Induced Constraints

The first mission induced constraint is the minimal spatial resolution p_{min} that is required by the task. The minimal spatial resolution directly yields the constraint on the altitude above ground level as

$$h_{max} = \frac{p_x}{2\tan\left(\frac{\alpha}{2}\right) p_{min}} \tag{55}$$

The second mission induced constraint can have two forms. The first one, which is used by Di Franco et al,[60] defines a minimal overlap ratio o_y between frames. This definition is useful for image stitching algorithms for which an overlap of around 30% is needed. Given the advancement per frame in Equation(53), the overlap ratio is given as

$$o_y = 1 - \frac{\Delta y}{y} \tag{56}$$

Other image processing algorithms might require another expression for the advancement constraint. For this second expression, the requirement is that any pixel or feature should be captured at least $F \in \mathbb{N}$ times. This parameter describing the frames per pixel/feature can be expressed as $F = \frac{y}{\Delta y}$.

These two definitions constrain the advancement per frame to

$$\Delta y_{max} = y(1 - o_{y,min}) \quad \vee \quad \Delta y_{max} = \frac{y}{F_{min}} \tag{57}$$

resulting in a constraint on the velocity as

$$v_{max} = \frac{2\tan\left(\frac{\alpha}{2}\right) f_r (1 - o_{y,min})}{r} h \quad \vee \quad v_{max} = \frac{2\tan\left(\frac{\alpha}{2}\right) f_r}{r F_{min}} h. \tag{58}$$

In the above, v_{max} is calculated using F_{min}. If an overlap based representation is of interest, a corresponding real valued $F_{min} = \frac{1}{1-o_{y,min}}$ can be computed.

B. Computational Load

Given the previous derivations, an approximation on the computational load based on the aircraft velocity and altitude can be made. Given the assumption that the information is proportional to the area, the information gain can be written as

$$\Delta I \propto \Delta A \tag{59}$$

with ΔA describing the previously unprocessed area. From the unprocessed area per second defined by $\Delta A = f_r x \Delta y$, the information gain relation can be rephrased as

$$\Delta I \propto 2\tan\left(\frac{\alpha}{2}\right) h v, \tag{60}$$

meaning that the information gain over time scales linearly with the altitude h and velocity v. If the computational load of the mission algorithm scales linearly with information gain, it can be deduced that computational load follows $\mathscr{L} \propto hv$.

Given this relation, the computational hardware should be chosen to have a computational load below 100% when flying at h^* with v^*, such that it is not over-provisioned but can handle each scenario. v^* is the minimum of v_{max} in

Equation (58) and the maximum possible velocity of the aircraft; and h^* is the minimum of h_{max} in Equation (55) and the maximal allowed flight altitude. Therefore, if the computational load at h^* with v^* is $\mathscr{L}^*$, the computational load for the mission algorithms at any altitude and velocity is calculated through

$$\mathscr{L}_{mission}(h,v) = \frac{hv}{h^*v^*}(\mathscr{L}^* - \mathscr{L}_{flight}), \tag{61}$$

yielding a total computational load as

$$\mathscr{L}(h,v) = \mathscr{L}_{flight} + \frac{hv}{h^*v^*}(\mathscr{L}^* - \mathscr{L}_{flight}). \tag{62}$$

The mapping to computational power consumption of the avionics, $P_{computation}$, is hardware dependent. This is especially so when having heterogeneous computational hardware, e.g. with CPU and GPU, where additional load mapping to the devices is necessary. Figure 10 shows an example profiling of a computational board, specifically the NVIDIA Tegra K1. The details of profiling of computational hardware is out of scope for this work.

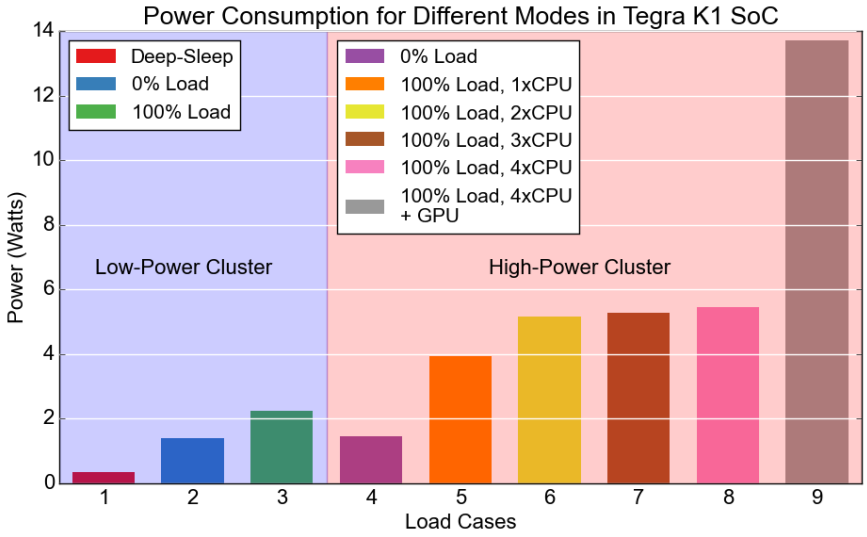

Figure 10: NVIDIA Tegra K1 power consumption depending on computational load of different modes.

VI. Summary and Future Work

This paper described an integrated power model for a solar-powered, computationally-intensive unmanned aircraft that included power models for solar generation, aircraft propulsion, and avionics. These power consumption and generation models were described, derived, and integrated into a cohesive system-wide aircraft power model that was presented in the form of a systemic flow diagram. Power balance expressions were imposed based on temporal and physical constraints.

For future work, the integrate power model will be experimentally validated as well as used for aircraft design and optimization. Parameters for the UIUC-TUM Solar Flyer from existing ground and flight test data will be quantified and incorporated into the model. Simulation will then be performed and compared to flight test results. The fidelity of the integrated power model will be analyzed and any discrepancies will be used to further refine and enhance the model.

Acknowledgments

The material presented in this paper is based upon work supported by the National Science Foundation (NSF) under grant number CNS-1646383. Marco Caccamo was also supported by an Alexander von Humboldt Professorship endowed by the German Federal Ministry of Education and Research. Any opinions, findings, and conclusions or recommendations expressed in this publication are those of the authors and do not necessarily reflect the views of the NSF.

References

[1]"Altavian," http://www.altavian.com/, Accessed May 2020.

[2]Precision Hawk, "Precision Agriculture, Commercial UAV and Farm Drones," http://precisionhawk.com/, Accessed May 2020.

[3]MicroPilot, "MicroPilot - MP-Vision," http://www.micropilot.com/products-mp-visione.htm, Accessed May. 2015.

[4]Theile, M., Dantsker, O. D., Caccamo, M., and Yu, S., "uavAP: A Modular Autopilot Framework for UAVs," AIAA Paper 2020-3268, AIAA Aviation 2020 Forum, Virtual Event, Jun. 2020.

[5]Dantsker, O. D., Theile, M., Caccamo, M., and Mancuso, R., "Design, Development, and Initial Testing of a Computationally-Intensive, Long-Endurance Solar-Powered Unmanned Aircraft," AIAA Paper 2018-4217, AIAA Applied Aerodynamics Conference, Atlanta, GA, Jun. 2018.

[6]Dantsker, O. D., Theile, M., Caccamo, M., Yu, S., Vahora, M., and Mancuso, R., "Continued Development and Flight Testing of a Long-Endurance Solar-Powered Unmanned Aircraft: UIUC-TUM Solar Flyer," AIAA Paper 2020-0781, AIAA Scitech 2020 Forum, Orlando, FL, Jan. 2020.

[7]Real Time and Embedded System Laboratory, University of Illinois at Urbana-Champaign, "Solar-Powered Long-Endurance UAV for Real-Time Onboard Data Processing," http://rtsl-edge.cs.illinois.edu/UAV/, Accessed Jan. 2018.

[8]Dantsker, O. D., Imtiaz, S., and Caccamo, M., "Electric Propulsion System Optimization for a Long-Endurance and Solar-Powered Unmanned Aircraft," AIAA Paper 2019-4486, AIAA/IEEE Electric Aircraft Technology Symposium, Indianapolis, Indiana, Aug. 2019.

[9]Dantsker, O. D., Imtiaz, S., and Caccamo, M., "Propulsion System Design, Optimization, Simulation, and Testing for a Long-Endurance Solar-Powered Unmanned Aircraft," AIAA Propulsion and Energy Forum 2020, Virtual Event, Aug. 2020.

[10]Green, C. R. and McDonald, R. A., "Modeling and Test of the Efficiency of Electronic Speed Controllers for Brushless DC Motors," AIAA Paper 2015-3191, AIAA Aviation Forum, Dallas, TX, Jun. 2015.

[11]McCrink, M. H. and Gregory, J. W., "Blade Element Momentum Modeling for Low-Re Small UAS Electric Propulsion Systems," AIAA Paper 2015-3191, AIAA Aviation Forum, Dallas, TX, Jun. 2015.

[12]Lundstrom, D., Amadori, K., and Krus, P., "Validation of Models for Small Scale Electric Propulsion Systems," AIAA Paper 2010-483, AIAA Aerospace Sciences Meeting, Orlando, FL, Jan. 2010.

[13]Ostler, J. and Bowman, W., "Flight Testing of Small, Electric Powered Unmanned Aerial Vehicles," U.S. Air Force T&E Days Conferences, American Institute of Aeronautics and Astronautics, Dec. 2005.

[14]Lee, J. S. and Yu, K. H., "Optimal Path Planning of Solar-Powered UAV Using Gravitational Potential Energy," *IEEE Transactions on Aerospace and Electronic Systems*, Vol. 53, No. 3, Jun. 2017, pp. 1442–1451.

[15]Grano-Romero, C., García-Juárez, M., Guerrero-Castellanos, J. F., Guerrero-Sánchez, W. F., Ambrosio-Lázaro, R. C., and Mino-Aguilar, G., "Modeling and control of a fixed-wing UAV powered by solar energy: An electric array reconfiguration approach," *2016 13th International Conference on Power Electronics (CIEP)*, Jun. 2016, pp. 52–57.

[16]Gao, X.-Z., Hou, Z.-X., Guo, Z., Liu, J.-X., and Chen, X.-Q., "Energy management strategy for solar-powered high-altitude long-endurance aircraft," *Energy Conversion and Management*, Vol. 70, No. Supplement C, 2013, pp. 20 – 30.

[17]Hosseini, S., Dai, R., and Mesbahi, M., "Optimal path planning and power allocation for a long endurance solar-powered UAV," *2013 American Control Conference*, Jun. 2013, pp. 2588–2593.

[18]B. Lee, B., Park, P., Kim, C., Yang, S., and Ahn, S., "Power managements of a hybrid electric propulsion system for UAVs," *Journal of Mechanical Science and Technology*, Vol. 26, No. 8, Aug 2012, pp. 2291–2299.

[19]Gong, A., MacNeill, R., and Verstraete, D., "Performance Testing and Modeling of a Brushless DC Motor, Electronic Speed Controller and Propeller for a Small UAV," AIAA Paper 2018-4584, AIAA Propulsion and Energy Forum, Cincinnati, OH, Jul. 2018.

[20]Gong, A. and Verstraete, D., "Experimental Testing of Electronic Speed Controllers for UAVs," AIAA Paper 2017-4955, AIAA/SAE/ASEE Joint Propulsion Conference, Atlanta, GA, Jul. 2017.

[21]Gong, A., Maunder, H., and Verstraete, D., "Development of an in-fight thrust measurement system for UAVs," AIAA Paper 2017-5092, AIAA/SAE/ASEE Joint Propulsion Conference, Atlanta, GA, Jul. 2017.

[22]Karabetsky, D., "Solar rechargeable airplane: Power system optimization," *2016 4th International Conference on Methods and Systems of Navigation and Motion Control (MSNMC)*, Oct. 2016, pp. 218–220.

[23]Park, H. B., Lee, J. S., and Yu, K. H., "Flight evaluation of solar powered unmanned flying vehicle using ground testbed," *2015 15th International Conference on Control, Automation and Systems (ICCAS)*, Oct. 2015, pp. 871–874.

[24]Lindahl, P., Moog, E., and Shaw, S. R., "Simulation, Design, and Validation of an UAV SOFC Propulsion System," *IEEE Transactions on Aerospace and Electronic Systems*, Vol. 48, No. 3, Jul. 2012, pp. 2582–2593.

[25]Brandt, J. B. and Selig, M. S., "Propeller Performance Data at Low Reynolds Numbers," AIAA Paper 2011-1255, AIAA Aerospace Sciences Meeting, Orlando, FL, Jan. 2011.

[26]Shiau, J. K., Ma, D. M., Chiu, C. W., and Shie, J. R., "Optimal Sizing and Cruise Speed Determination for a Solar-Powered Airplane," *AIAA Journal of Aircraft*, Vol. 47, No. 2, Mar. 2010, pp. 622–629.

[27]Khan, W. and Nahon, M., "Modeling dynamics of agile fixed-wing UAVs for real-time applications," *2016 International Conference on Unmanned Aircraft Systems (ICUAS)*, Jun. 2016, pp. 1303–1312.

[28]Selig, M. S., "Real-Time Flight Simulation of Highly Maneuverable Unmanned Aerial Vehicles," *Journal of Aircraft*, Vol. 51, No. 6, Nov.-Dec. 2014, pp. 1705–1725.

[29]Johnson, E. N. and Mishra, S., "Flight Simulation for the Development of an Experimental UAV," AIAA Paper 2002-4975, AIAA Modeling and Simulation Technologies Conference and Exhibit, Monterey, CA, Aug. 2002.

[30]FlightGear Flight Simulator, "FlightGear," http://www.flightgear.org, Accessed Oct. 2017.

[31]Rayleigh, L., "The Soaring of Birds," *Nature*, Vol. 27, Apr. 1883, pp. 534–535.

[32]Hendriks, F., *Dynamic Soaring*, Ph.D. thesis, Univ. of CA, Los Angles, CA, 1972.

[33]Barnes, J. P., "How Flies the Albatross—The Flight Mechanics of Dynamic Soaring," *SAE Paper 2004-01-3088, Nov. 2004*.

[34]Sukumar, P. P. and Selig, M. S., "Dynamic Soaring of Sailplanes over Open Fields," *Journal of Aircraft*, Vol. 50, No. 5, Sep.-Oct. 2013, pp. 1420–1430.

[35]Woodbury, T., Dunn, C., and Valasek, J., "Autonomous Soaring Using Reinforcement Learning for Trajectory Generation," AIAA Paper 2014-0990, AIAA SciTech Forum, National Harbor, MD, Jan. 2014.

[36]Bird, J. J. and Langelaan, J. W., "Optimal Speed Scheduling for Hybrid Solar Aircraft with Arrival Time Condition," AIAA Paper 2019-1421, AIAA SciTech Forum, San Diego, CA, Jan. 2019.

[37]Shiau, J. K., Ma, D. M., Yang, P. Y., Wang, G. F., and Gong, J. H., "Design of a Solar Power Management System for an Experimental UAV," *IEEE Transactions on Aerospace and Electronic Systems*, Vol. 45, No. 4, Oct. 2009, pp. 1350–1360.

[38]Iqbal, M., "An Introduction to Solar Radiation," 1983.

[39]Michalsky, J. J., "The Astronomical Almanac's algorithm for approximate solar position (1950–2050)," *Solar Energy*, Vol. 40.

[40]Meeus, J., *Astronomical Algorithms, 2nd Edition*, Willmann-Bell, Inc., Richmond, VA, 1999.

[41]Kumar, L., Skidmore, A. K., and Knowles, E., "Modelling topographic variation in solar radiation in a GIS environment," *International Journal of Geographical Information Science*, Vol. 11, No. 5, 1997, pp. 475–497.

[42]Jenkins, A., "The Sun's position in the sky," *European Journal of Physics*, Vol. 34, No. 3, Mar. 2013, pp. 633–652.

[43]Reda, I. and Andreas, A., "Solar Position Algorithm for Solar Radiation Applications," Tech. rep., US Department of Energy, National Renewable Energy Laboratory, NREL/TP-560-34302, 2008.

[44]Walker, C. and Vaucher, G., "Atmospheric Renewable Energy Research,Volume 5 (Solar Radiation Flux Model)," Tech. rep., US Army Research Laboratory, ARL-TR-8155, 2017.

[45]Khatib, T. and Elmenreich, W., *Modeling of Photovoltaic Systems Using MATLAB: Simplified Green Codes*, John Wiley & Sons, Inc., Hoboken, NJ, 2016.

[46]Hebeler, F., "Solar Radiation," https://www.mathworks.com/matlabcentral/fileexchange/19791-solar-radiation, 2020.

[47]Alta Devices, "Technology Brief - Single Junction," https://www.altadevices.com/wp-content/uploads/2018/01/tb-single-junction-1712-001.pdf.

[48]McCormick, B. W., *Aerodynamics, Aeronautics, and Flight Mechanics, 2nd Edition*, John Wiley & Sons, Inc., Hoboken, NJ, 1994.

[49]Dantsker, O. D., Theile, M., and Caccamo, M., "A High-Fidelity, Low-Order Propulsion Power Model for Fixed-Wing Electric Unmanned Aircraft," AIAA Paper 2018-5009, AIAA/IEEE Electric Aircraft Technologies Symposium, Cincinnati, OH, Jul. 2018.

[50]Ol, M., Zeune, C., and Logan, M., "Analytical/Experimental Comparison for Small Electric Unmanned Air Vehicle Propellers," *26th AIAA Applied Aerodynamics Conference*, American Institute of Aeronautics and Astronautics, Reston, VA, 8 2008.

[51]Dantsker, O. D., Caccamo, M., Deters, R. W., and Selig, M. S., "Performance Testing of Aero-Naut CAM Folding Propellers," AIAA Paper 2020-2762, AIAA Aviation 2020 Forum, Virtual Event, Jun. 2020.

[52]UIUC Applied Aerodynamics Group, "UIUC Propeller Data Site," http://m-selig.ae.illinois.edu/props/propDB.html.

[53]O. Dantsker and R. Mancuso and M. Vahora, "Unmanned Aerial Vehicle Database," http://uavdb.org/.

[54]Drela, M., "First-Order DC Electric Motor Model," http://web.mit.edu/drela/Public/web/qprop/motor1_theory.pdf, Accessed May 2020.

[55]Drela, M., "Second-Order DC Electric Motor Model," http://web.mit.edu/drela/Public/web/qprop/motor2_theory.pdf, Accessed May 2020.

[56]Landing Products Inc., "APC Propeller Performance Data," https://www.apcprop.com/technical-information/performance-data/, Accessed May 2020.

[57]Mark Drela, "QPROP," http://web.mit.edu/drela/Public/web/qprop/, Accessed Jan. 2019.

[58]Martin Hepperle, "Java Prop," https://www.mh-aerotools.de/airfoils/javaprop.htm, Accessed Jun. 2019.

[59]Theile, M., Dantsker, O. D., Nai, R., and Caccamo, M., "uavEE: A Modular, Power-Aware Emulation Environment for Rapid Prototyping and Testing of UAVs," IEEE International Conference on Embedded and Real-Time Computing Systems and Applications, Hakodate, Japan, Aug. 2018.

[60]Franco, C. D. and Buttazzo, G., "Energy-Aware Coverage Path Planning of UAVs," *2015 IEEE International Conference on Autonomous Robot Systems and Competitions*, 2015, pp. 111–117.